Cu and Co Nanoparticle Co-decorated N-doped Graphene Nanosheets: A High Efficiency Bifunctional Electrocatalyst for Rechargeable Zn-Air Batteries

Peitao Liu[a]‡, YatingHu[b]‡, Xiaokai Liu[a],Tongtong Wang[a], Pinxian Xi[c], Shibo Xi[d], Daqiang Gao[a*]and John Wang[b*].

[a]P. Liu, X. Liu,T. Wang, Prof. D. Gao
Key Laboratory for Magnetism and Magnetic Materials of MOE, Key Laboratory of Special Function Materials and Structure Design of MOE, Lanzhou University, Lanzhou 730000, P. R. China
Email: gaodq@lzu.edu.cn

[b]Y. Hu, Prof. J. Wang
Department of Material Science and Engineering, National University of Singapore, Engineering Drive 3, 117575, Singapore
Email: msewangj@nus.edu.sg

[c]Prof. P. Xi
Key Laboratory of Nonferrous Metal Chemistry and Resources Utilization of Gansu Province and The Research Center of Biomedical Nanotechnology, Lanzhou University, Lanzhou, 730000, P. R. China

[d]Dr. S. Xi
Institute of Chemical and Engineering Sciences, A*STAR, 1 Pesek Road, Jurong Island, 627833, Singapore

‡ These two athors contribution equall to this work.

Experimental Section

Preparation of CuCo@N-C, Co@N-C and Cu@N-C: In a typical procedure, 0.01 mol $CoCl_2 \cdot 6H_2O$, 0.01 mol $CuCl_2 \cdot 2H_2O$ and 4 g $C_2H_4N_4$ were dissolved in 30 ml ethanol under vigorously stirring. After that, the homogeneous miscible liquid was transferred into an oven at 90 °C for overnight. The precursor after dry was thermally treated at 800 °C in an argon atmosphere for 3 h. For comparison, Co@N-C and Cu@N-C were synthesized by the same method, but excluding Cu source or Co source in the process. N-C was also prepared by the same method, but excluding Cu and Co source added in the process.

Materials Characterizations: X-ray diffractometer (XRD) patterns were collected by using a Rigaku D/Max-2400 diffractometer with Cu Ka radiation (λ = 1.54178 Å). Transmission electron microscopy (TEM) studies were performed on Tecnai G2 F30 Field Emission Transmission Electron Microscope. The chemical states and bonding characteristics were analyzed by X-ray photoelectron spectroscopy (XPS; Kratos AXIS Ultra). Raman spectrum was measured on a Jobin-Yvon HR80 spectrometer at room temperature. N_2 adsorption/desorption isotherms were collected at 80 °C by using a Micromeritics ASAP 2020 V403. X-ray absorption near edge structures (XANES) and extended X-ray absorption fine structures (EXAFS) were measured in the vicinity of the Co and Cu K edge at the XAFCA beamline of the Singapore Synchrotron Light Source (SSLS), Singapore.

Calculation details：We used a computational code of Vienna *ab initio* simulation package (VASP) for DFT calculations. The standard generalized-gradient approximation (GGA) was adopted for the exchange-correlation potential. The energy cutoff of the plane waves used for expanding electronic wave functions is 400 eV. A Monkhorst–Pack k-point mesh of 4×4×4 was used for geometry optimization and electronic property calculations. Both atomic positions and cell parameters were optimized until the residual forces were below 0.01 eV/Å.

Electrochemical Measurements: The OER and ORR electrochemical process were recorded at room temperature (25 ± 0.5 °C) on a CHI 760e Electrochemical Workstation (CHI Instruments, Shanghai Chenhua Instrument Corporation, China) with three-electrode system: as-prepared samples on a Platinum carbon electrode or a rotating ring-disk electrode (RRDE) used as the working electrode, a saturated Ag/AgCl reference electrode and a platinum-foil counter electrode. The measured potentials (vs Ag/AgCl) in this work were converted to a reversible hydrogen electrode (RHE) and iR corrected according to the Nernst equation ($E_{\mathrm{RHE}} = E_{\mathrm{Ag/AgCl}} + 0.197 + 0.059\ \mathrm{pH}$). As for the ORR, the catalytic ink was prepared by homogeneously dispersed 3 mg catalysts in 1470 μL N,N-Dimethylformamide (DMF) and 30 μL Nafion. Then, the catalytic ink was dropped onto the rotating disk working electrode (RDE) at a loading amount of 0.2 mg/cm^2 and dried at room temperature. All the ORR properties were tested on RRDE at 1600 rpm in O_2-saturated 0.1 M KOH solution with the varied rotating speeds.

Zn-Air Batteries test: A home-made rechargeable ZABs was assembled using polished zinc plate as the anode, a carbon fiber paper (CFP) with the catalyst (loading amount of 2 mg cm^{-2}) as air cathode and 6 M KOH with 0.2 M zinc acetate solution as electrolyte according to the previous work. As for micro-solid-state ZABs were assembled with CuCo@N-C as air cathode, polished Zn plate as an anode and alkaline hydrogel polymer as the electrolyte. The battery performance was recorded on a potentiostat (CHI 760E, CH Instrument Co.) and LAND testing system. For comparison, the 20 wt% Pt/C based ZAB was also studied under the same conditions.

Calculation of electron transferred number (n) for ORR

The number of electron transfer per O_2 participate in oxygen reduction can be determined by Koutechy-Levich equation:

$$1/j = 1/j_k + 1/B\omega^{1/2} \tag{5}$$

where j_k is the kinetic current and ω is the electrode rotating rate. B is determined from the slope of the Koutechy-Levich (K-L) plots based on the Levich equation below:

$$B = 0.2nF(D_{O_2})^{2/3}\upsilon^{-1/6}C_{O_2} \tag{6}$$

where n represents the transferred electron number per oxygen molecule. F is Faraday constant (F = 96485 C mol^{-1}). D_{O_2} is the diffusion coefficient of O_2 in 0.1 M KOH (D_{O_2} = 1.9 × 10^{-5} cm^2 s^{-1}). υ is the kinetic viscosity (υ = 0.01 cm^2 s^{-1}). C_{O_2} is the bulk concentration of O_2 (C_{O_2} = 1.2 × 10^{-6} mol cm^{-3}). The constant 0.2 is adopted when the rotation speed is expressed in rpm.

For the Rotating Ring-Disk Electrodes measurements, the $\%HO_2^-$ and transfer number (n) were determined by the followed equations:

$$\%HO_2^- = 200\frac{I_r/N}{I_d + I_r/N} \tag{7}$$

$$n = 4\frac{I_d}{I_d + I_r/N} \tag{8}$$

where I_d is disk current, I_r is ring current and N is current collection efficiency of the Pt ring. N was determined to be 0.40.

Calculation of specific capacity and energy density for Zn-air batteries

The specific capacity was calculated by the equation below:

$$\textit{Specific Capacity} = I \times t/m_{Zn} \tag{9}$$

The energy density was calculated by the equation below:

$$\textit{Energy Density} = I \times t \times V/m_{Zn} \tag{10}$$

Where I denotes Current, t denotes the service hours, V denotes the average discharge voltage, and m_{Zn} denotes the weight of consumed zinc.

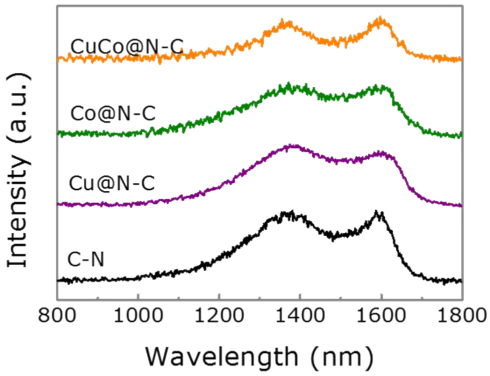

Figure S1. The Raman spectra of catalysts CuCo@N-C, Co@N-C, Cu@N-C and N-C.

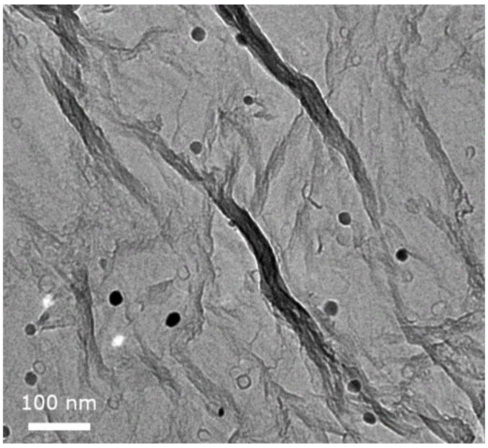

Figure S2. TEM image of catalyst CuCo@N-C.

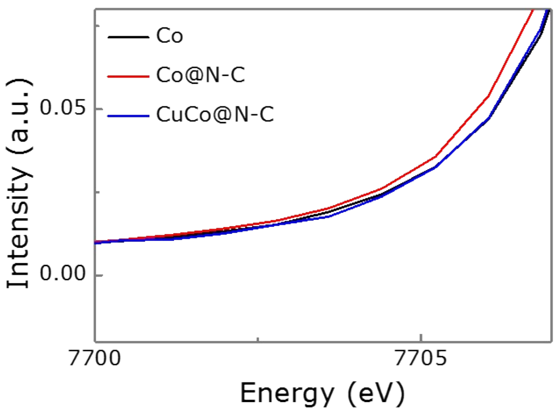

Figure S3. XANES spectrum of Co foil, Co@N-C and CuCo@N-C.

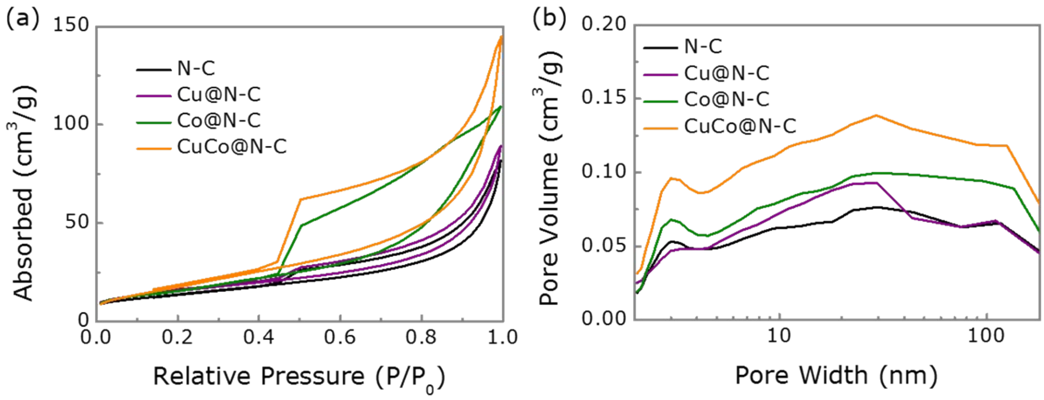

Figure S4. (a) BET plots and (b) pore width of CuCo@N-C, Co@N-C, Cu@N-C and N-C.

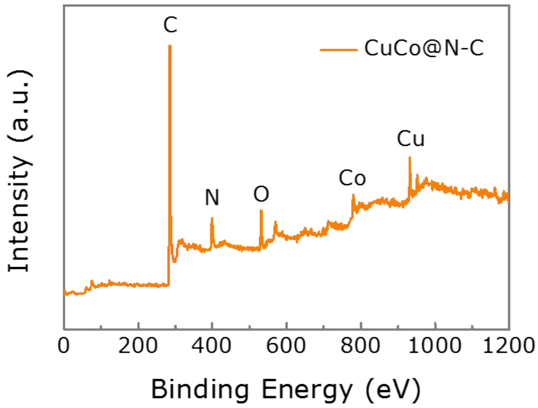

Figure S5. The XPS spectrum of CuCo@N-C.

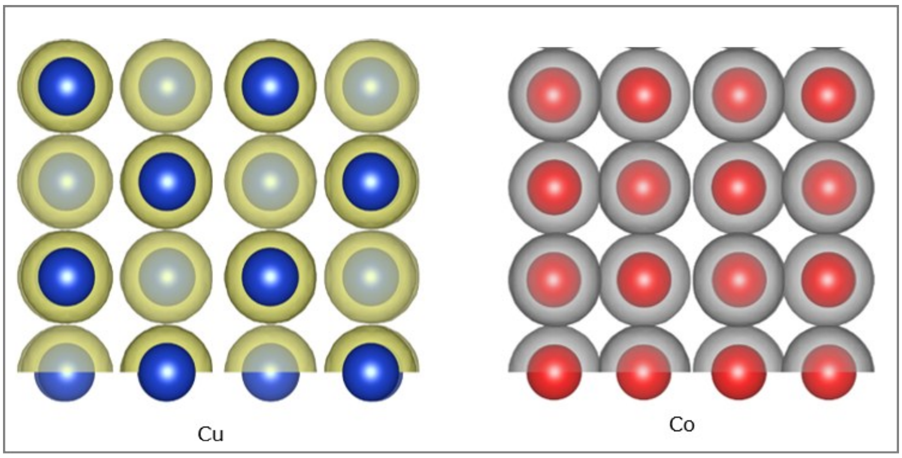

Figure S6. The charge density of Cu and Co with the isosurface value of 0.05 e/bohr^3.

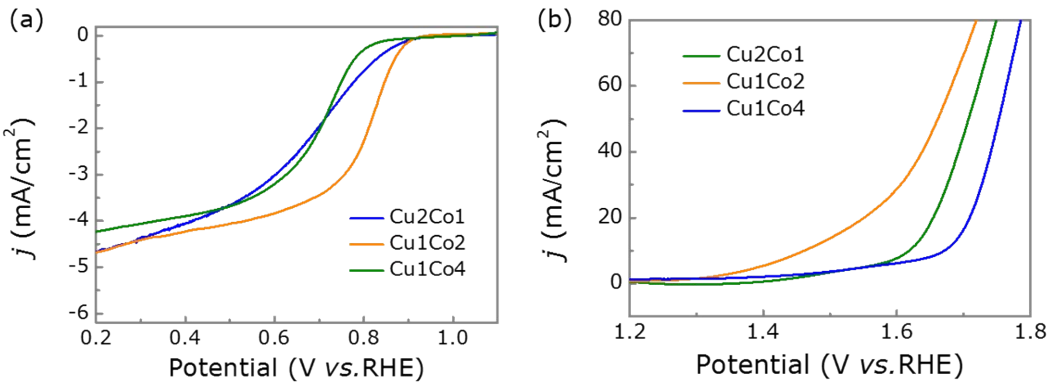

Figure S7. (a) LSV polarization curves of ORR for all the catalysts (Cu : Co= 2 : 1, 1 : 2 and 1 : 4, respectively.) at 1600 rpm. (b) LSV polarization curves of OER for all the catalysts (Cu : Co= 2 : 1, 1 : 2 and 1 : 4, respectively.).

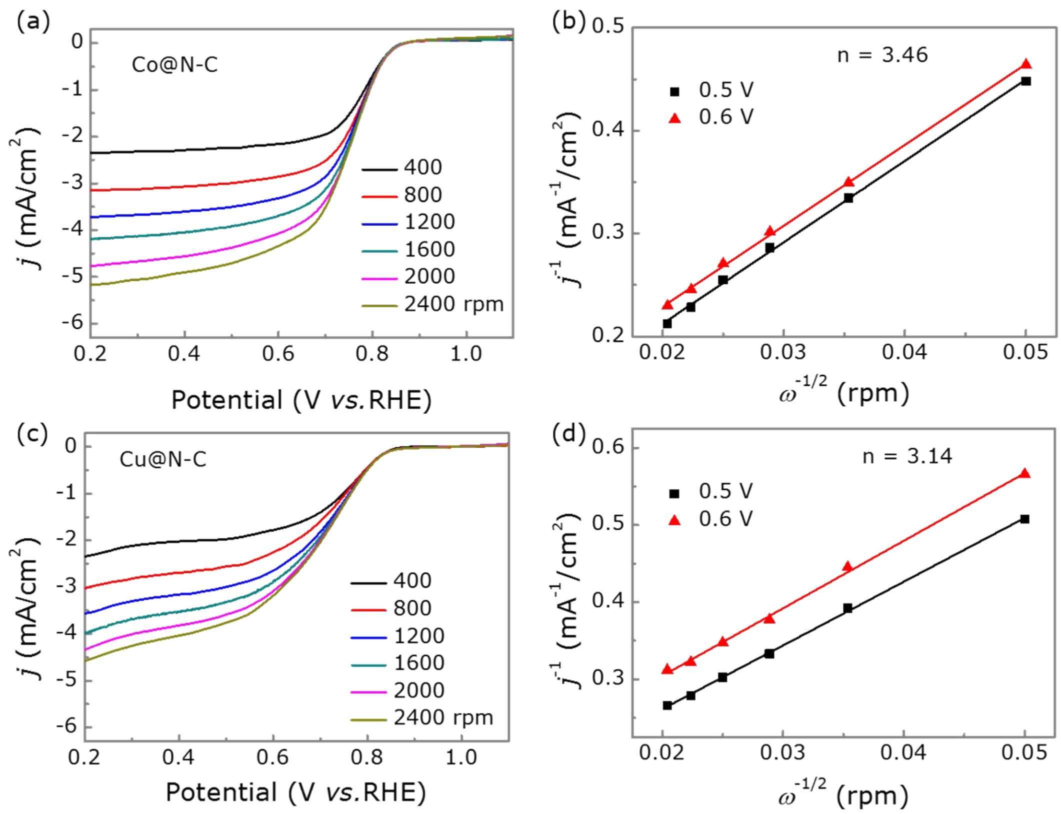

Figure S8. (a) LSV curves of ORR for Co@N-C at different rotation speeds and (b) the corresponding Koutecky–Levich plots. (c) LSV curves of ORR for Cu@N-C at different rotation speeds and (d) the corresponding Koutecky–Levich plots.

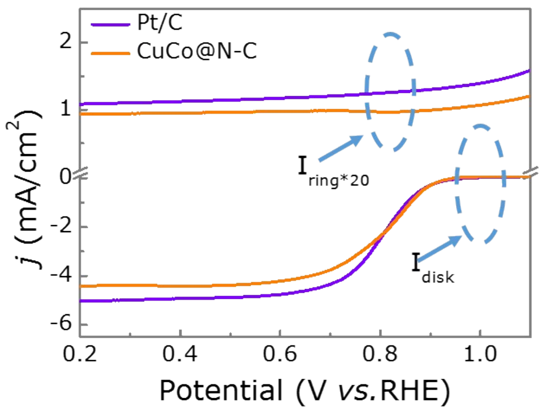

Figure S9. The RRDE curves for CuCo@N-C and Pt/C in O_2 saturated 0.1 M KOH at 1600 rpm.

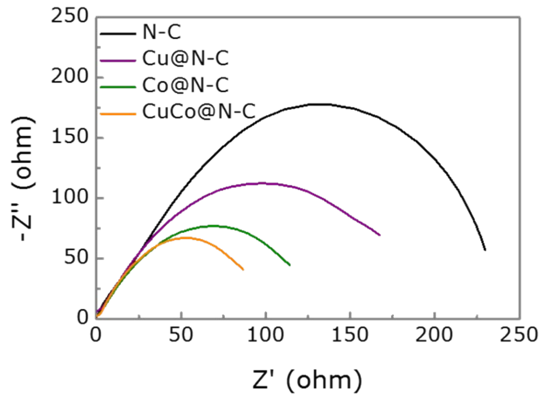

Figure S10. EIS cruves of catalysts CuCo@N-C, Co@N-C, Cu@N-C and N-C.

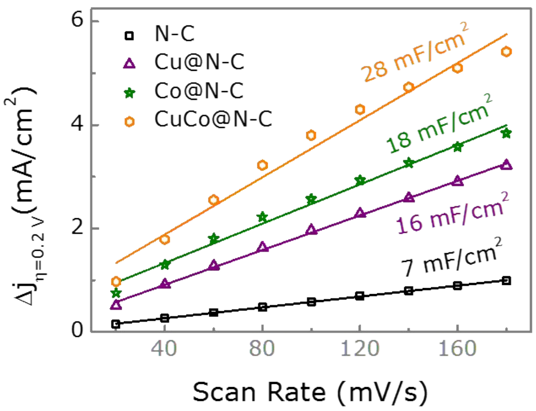

Figure S11. ECSA results of catalysts CuCo@N-C, Co@N-C, Cu@N-C and N-C.

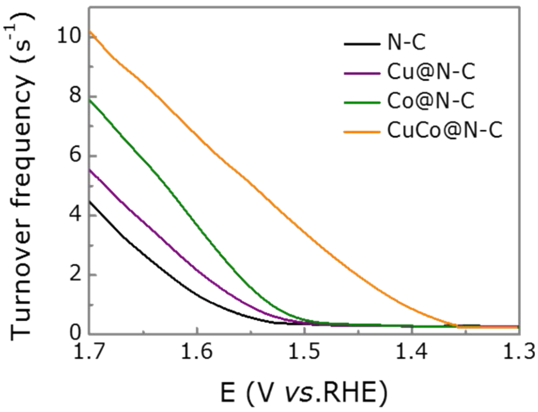

Figure S12. TOF results of catalysts CuCo@N-C, Co@N-C, Cu@N-C and N-C.

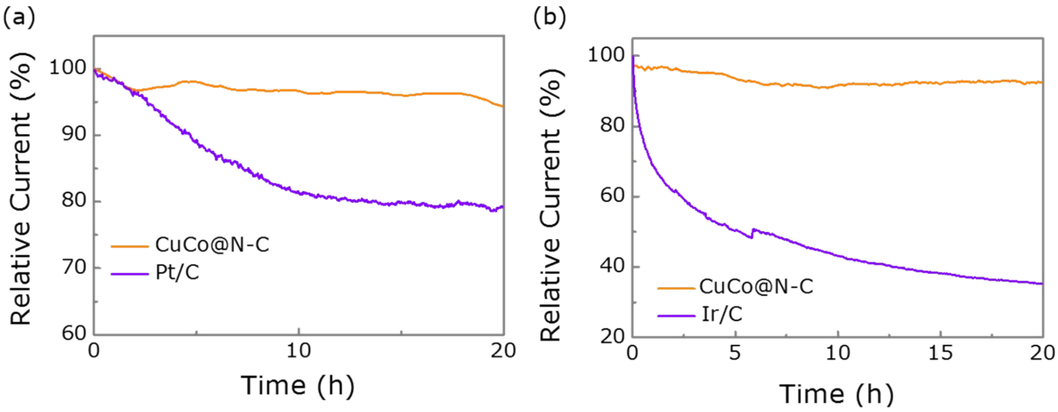

Figure S13. (a) The chronopotentiometric response of ORR for catalyst CuCo@N-Cand Pt/C (20%) at aconstant voltage of 0.7 V *vs.* RHE. (b) The chronopotentiometric response of OER for CuCo@N-C and Ir/C (20%) at aconstant voltage of 1.50 V *vs.* RHE.

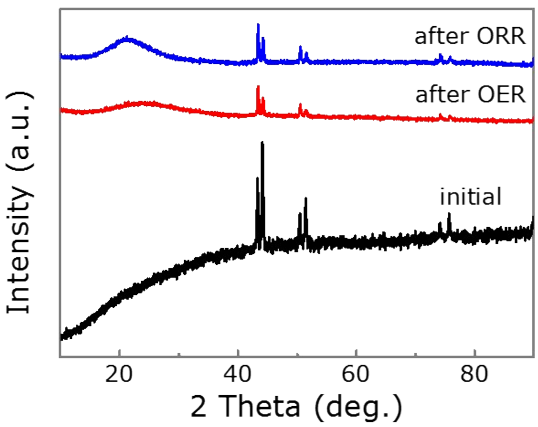

Figure S14. XRD results of CuCo@N-C after the stability test.

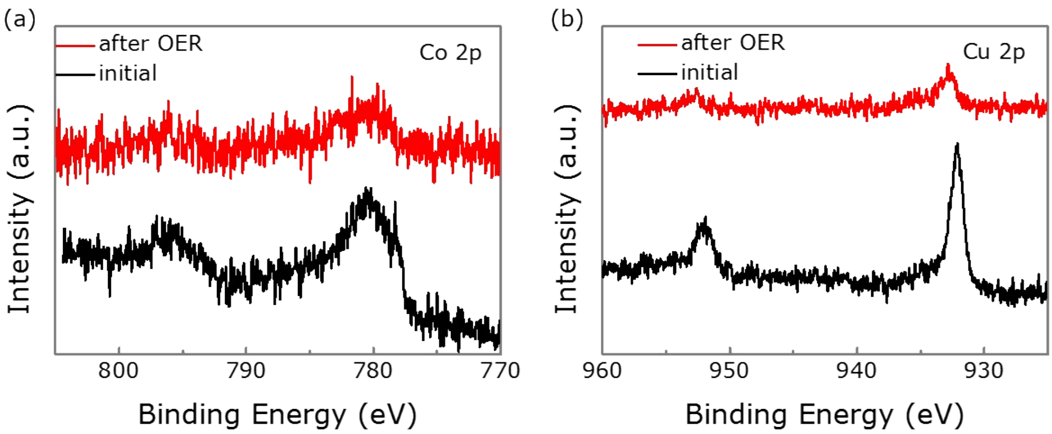

Figure S15. XPS results of CuCo@N-C after the OER test.

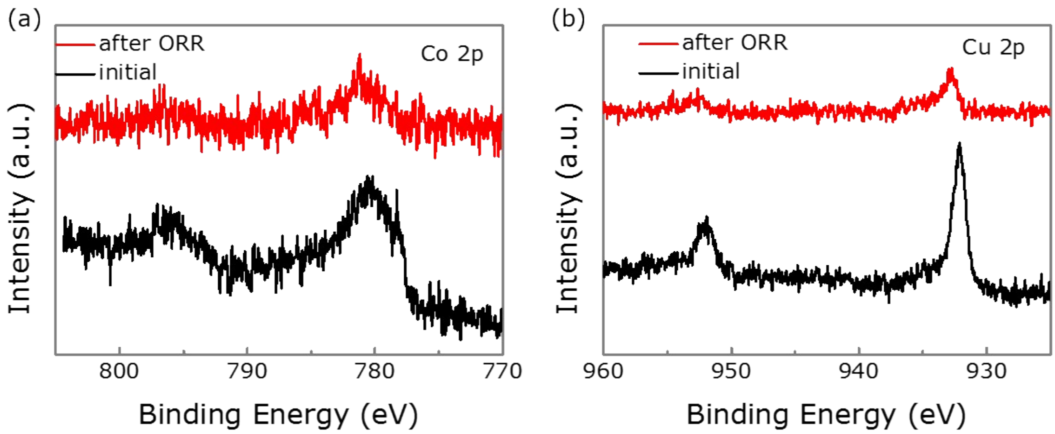

Figure S16. XPS results of CuCo@N-C after the ORR test.

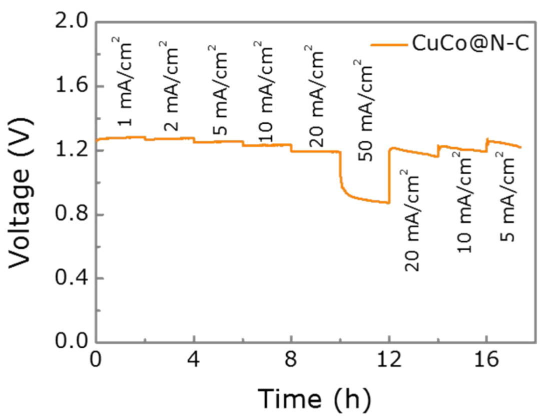

Figure S17. Discharge curves of the CuCo@N-C based ZABs at different current densities.

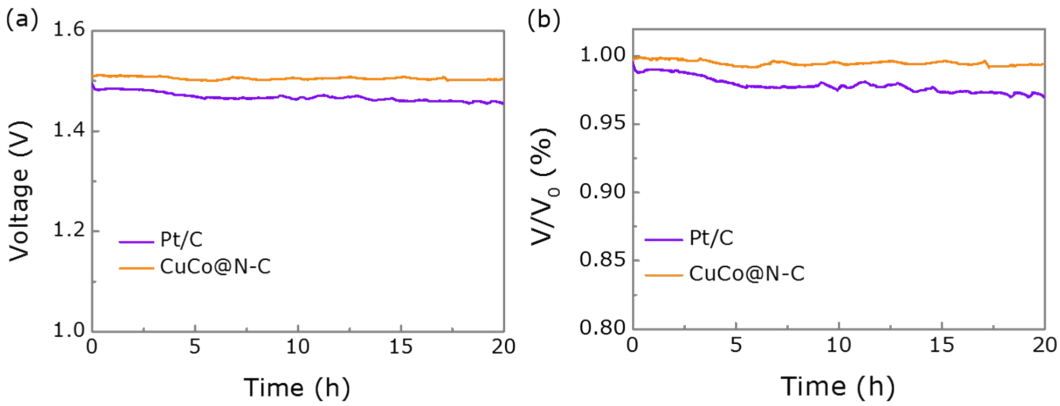

Figure S18. (a) The Open circuit voltage of Pt/C and CuCo@N-C. (b)The precentage of V/V_0 for Pt/C and CuCo@N-C.

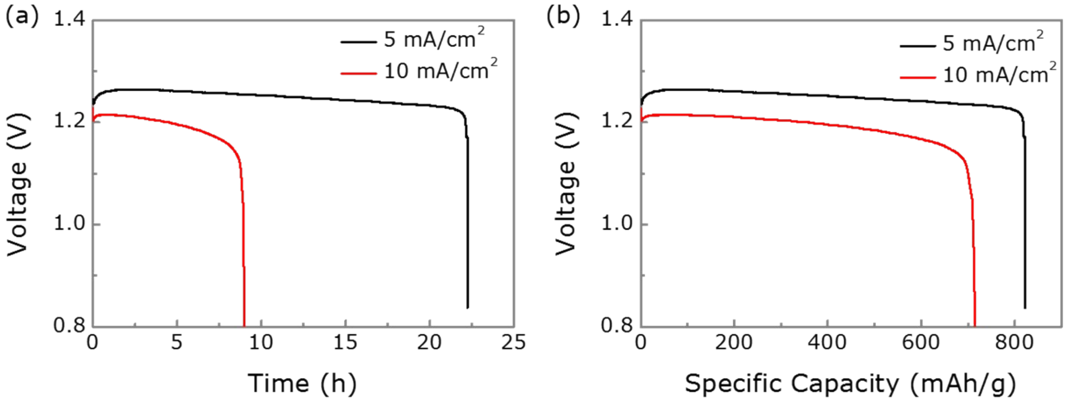

Figure S19. (a) Discharge curves at the current density of 5 mA/cm^2, 10 mA/cm^2 and (d) the corresponding specific capacities of the CuCo@N-C based battery, respectively.

Figure S20. Schematic representation of the micro-solid-like ZABs based on CuCo@N-C air cathode.

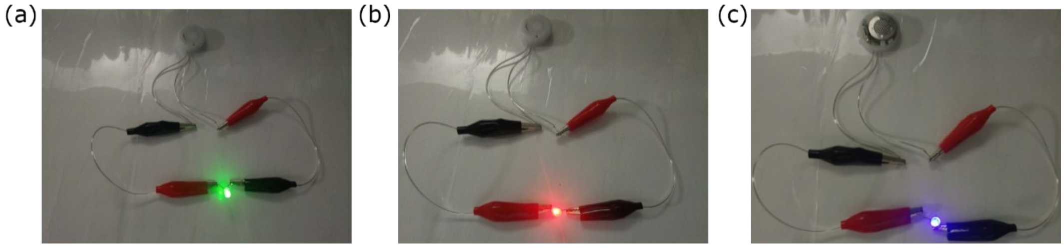

Figure S21. (a), (b) and (c) The photograph of a blue, green and red LED powered by two tandem all-solid-state ZABs.

Table S1. The E ($E = E_{j=10} - E_{1/2}$) value of our work and others comparison with CuCo compounds (oxides, hydroxides, nitrides, phosphides) catalysts.

Catalysts	$E_{j=10}$/V (10 mA/cm^2)	$E_{1/2}$/V	E/V ($E_{j=10} - E_{1/2}$)	Ref.
N-C	1.71	0.60	1.11	This work
Cu@N-C	1.68	0.69	0.99	This work
Co@N-C	1.65	0.75	0.90	This work
CuCo@N-C	1.46	0.81	0.65	This work
50% Pt/C + 50% Ir/C	1.56	0.78	0.78	This work
$CuCo_2O_4$@C	1.56	~	~	[1]
$CuCo_2O_4$-SSM	~	0.80	~	[2]
Co_3O_4@C-MWCNTS	1.55	0.81	0.74	[3]
Co_3O_4/NRGO	1.65	0.82	0.83	[4]
Co-N_x/C NRA	1.53	0.88	0.65	[5]
Co_2P@NPC	1.56	0.83	0.73	[6]
Co_3ZnC/Co	1.60	0.81	0.79	[7]
Cu@CoFe	1.47	~	~	[8]
Co@Co_3O_4/NC	1.65	0.80	0.85	[9]
(Ni, Co)/CNT	1.43	0.74	0.69	[10]
Cu_2O-Cu	1.48	~	~	[11]
CoNC-CNF-1000	1.68	0.80	0.88	[12]
Co-NC@CoP-NC	1.47	0.78	0.69	[13]

Table S2. Comparison of the performances of ZABs of our work and other recently reported catalysts.

Catalysts	Electrolyte	Open-circuit potential (V)	Power density (mW/cm^2)	Ref.
Pt/C	6.0 M KOH	1.48	165	The work
CuCo@N-C	6.0 M KOH	1.51	170	The work
$CoIn_2S_4$/S-rGO	6.0 M KOH + 0.2 M $ZnCl_2$	1.42	133	14
Fe@C-NG/NCNTs	6.0 M KOH	1.37	101	15
FeN_x/C-700-20	6.0 M KOH	~	36	16
CoFe/N-GCT	~	1.43	203	17
$LaMnO_{3+\delta}$	6.0 M KOH	1.43	199	18
N,P-NC-1000	6.0 M KOH	1.48	146	19
CFZr(0.3)/rGO	6.0 M KOH	1.39	~	20
Ni_3Fe/N-S-CNTs	6.0 M KOH	~	180	21
FeNi-NC	6.0 M KOH + 0.2 M ZnO	~	81	22
CoNiFe-S MNS	6.0 M KOH + 0.2 M $ZnCl_2$	~	140	23
FeS/Fe_3C@N-S-C-800	6.0 M KOH + 0.2 M $Zn(Ac)_2$	1.43	65	24
Fe-N-CNBs-600	6.0 M KOH	1.53	257	25
Ni-Fe-MoN NTs	6.0 M KOH + 0.2 M $Zn(Ac)_2$	1.35	118	26
Co-MOF	6.0 M KOH + 0.2 M $Zn(Ac)_2$	1.33	86	27
$NiCo_2O_4$@N-OCNT	6.0 M KOH + 0.2 M $Zn(OAc)_2$	1.40	50	28
FeNC-S-Fe_xC/Fe	6.0 M KOH + 0.02 M $Zn(Ac)_2$	1.41	149	29
Co/Co3O4@PGS	6.0 M KOH + 0.2 M $Zn(Ac)_2$	1.45	118	30

Table S3. Comparison of the performances of solid-like ZABs our work and other recently reported catalysts.

Catalysts	Electrolyte	Open-circuit Voltage (V)	Power density (mW/cm^2)	Ref.
Pt/C	PVA glue	1.48	92.8	The work
CuCo@N-C	PVA glue	1.46	82.9	The work
CNT@POF	PVA glue	1.39	22.3	[31]
CoN_4/NG	PVA glue	~	28.0	[32]
NC-Co SA	PVA glue	1.41	20.9	[33]
NC-Co/CoN_x	~	1.40	41.5	[34]
CC-AC	PVA glue	1.37	52.3	[35]
N,S-CC	PVA glue	1.25	47	[36]

References

1 X. Wang, Y. Li, T. Jin, J. Meng, L. Jiao, M. Zhu, J. Chen, Electrospun Thin-Walled $CuCo_2O_4$@C Nanotubes as Bifunctional Oxygen Electrocatalysts for Rechargeable Zn-Air Batteries, *Nano lett*., 2017, **17**, 7989-7994.

2 A. Serov, N. I. Andersen, A. J. Roy, I. Matanovic, K. Artyushkova, P. Atanassov, $CuCo_2O_4$ ORR/OER Bi-Functional Catalyst: Influence of Synthetic Approach on Performance, *J. Electrochem. Soc.,* 2015, **162**, F449-F454.

3 X. Li, Y. Fang, X. Lin, M. Tian, X. An, Y. Fu, R. Li, J. Jin, J. Ma, MOF derived Co_3O_4 nanoparticles embedded in N-doped mesoporous carbon layer/MWCNT hybrids: extraordinary bi-functional electrocatalysts for OER and ORR, *J. Mater. Chem. A*, 2015, **3**, 17392-17402.

4 K. Kumar, C. Canaff, J. Rousseau, S. Arrii-Clacens, T. W. Napporn, A. Habrioux, K. B. Kokoh, Effect of the Oxide–Carbon Heterointerface on the Activity of Co_3O_4/NRGO Nanocomposites toward ORR and OER, *J. Phy. Chem. C*, 2016, **120**, 7949-7958.

5 I. S. Amiinu, X. Liu, Z. Pu, W. Li, Q. Li, J. Zhang, H. Tang, H. Zhang, S. Mu, From 3D ZIF Nanocrystals to Co-N_x/C Nanorod Array Electrocatalysts for ORR, OER, and Zn-Air Batteries, *Adv. Funct. Mater.*, 2018, **28**, 1704638.

6 J. Li, G. Liu, B. Liu, Z. Min, D. Qian, J. Jiang, J. Li, An extremely facile route to Co_2P encased in N,P-codoped carbon layers: Highly efficient bifunctional electrocatalysts for ORR and OER, *Int. J. Hydrogen Energy*, 2018, **43**, 1365-1374.

7 J. Su, G. Xia, R. Li, Y. Yang, J. Chen, R. Shi, P. Jiang, Q. Chen, Co_3ZnC/Co nano heterojunctions encapsulated in N-doped graphene layers derived from PBAs as highly efficient bi-functional OER and ORR electrocatalysts, *J. Mater. Chem. A*, 2016, **4**, 9204-9212.

8 L. Yu, H. Zhou, J. Sun, F. Qin, D. Luo, L. Xie, F. Yu, J. Bao, Y. Li, Y. Yu, S. Chen, Z. Ren, Hierarchical Cu@CoFe layered double hydroxide core-shell nanoarchitectures as bifunctional electrocatalysts for efficient overall water splitting, *Nano Energy*, 2017, **41**, 327-336.

9 A. Aijaz, J. Masa, C. Rosler, W. Xia, P. Weide, A. J. Botz, R. A. Fischer, W. Schuhmann, M. Muhler, Co@Co_3O_4 Encapsulated in Carbon Nanotube-Grafted Nitrogen-Doped Carbon Polyhedra as an Advanced Bifunctional Oxygen Electrode, *Angew. Chem. Int. Ed.*, 2016, **55**, 4087-4091.

10 N. Ma, Y. Jia, X. Yang, X. She, L. Zhang, Z. Peng, X. Yao, D. Yang, Seaweed biomass derived (Ni,Co)/CNT nanoaerogels: efficient bifunctional electrocatalysts for oxygen evolution and reduction reactions, *J. Mater. Chem. A*, 2016, **4**, 6376-6384.

11 H. Xu, J.-X. Feng, Y.-X. Tong, G.-R. Li, Cu_2O–Cu Hybrid Foams as High-Performance Electrocatalysts for Oxygen Evolution Reaction in Alkaline Media, *ACS Catal.*, 2016, **7**, 986-991.

12 W. Zhang, X. Yao, S. Zhou, X. Li, L. Li, Z. Yu, L. Gu, ZIF-8/ZIF-67-Derived Co-N_x-Embedded 1D Porous Carbon Nanofibers with Graphitic Carbon-Encased Co Nanoparticles as an Efficient Bifunctional Electrocatalyst, *Small*, 2018, **14**,

e1800423.

13 X. Li, Q. Jiang, S. Dou, L. Deng, J. Huo, S. Wang, ZIF-67-derived Co-NC@CoP-NC nanopolyhedra as an efficient bifunctional oxygen electrocatalyst, *J. Mater. Chem. A*, 2018, **4**, 15836-15840.

14 G. Fu, J. Wang, Y. Chen, Y. Liu, Y. Tang, J. B. Goodenough, J. M. Lee, Exploring Indium-Based Ternary Thiospinel as Conceivable High-Potential Air-Cathode for Rechargeable Zn-Air Batteries, *Adv. Energy Mater.*, 2018, **8**, 1802263.

15 Q. Wang, Y. Lei, Z. Chen, N. Wu, Y. Wang, B. Wang, Y. Wang, Fe/Fe_3C@C nanoparticles encapsulated in N-doped graphene–CNTs framework as an efficient bifunctional oxygen electrocatalyst for robust rechargeable Zn–air batteries, *J. Mater. Chem. A*, 2018, **6**, 516-526.

16 S. Han, X. Hu, J. Wang, X. Fang, Y. Zhu, Novel Route to Fe-Based Cathode as an Efficient Bifunctional Catalysts for Rechargeable Zn-Air Battery, *Adv. Energy Mater.*, 2018, **8**, 1800955.

17 X. Liu, L. Wang, P. Yu, C. Tian, F. Sun, J. Ma, W. Li, H. Fu, A Stable Bifunctional Catalyst for Rechargeable Zinc-Air Batteries: Iron-Cobalt Nanoparticles Embedded in a Nitrogen-Doped 3D Carbon Matrix, *Angew. Chem. Int. Ed.*, 2018, **57**, 16166-16170.

18 L. Kuai, E. Kan, W. Cao, M. Huttula, S. Ollikkala, T. Ahopelto, A.-P. Honkanen, S. Huotari, W. Wang, B. Geng, Mesoporous $LaMnO_3+\delta$ perovskite from spray−pyrolysis with superior performance for oxygen reduction reaction and Zn−air battery, *Nano Energy*, 2018, **43**, 81-90.

19 H. Luo, W.-J. Jiang, Y. Zhang, S. Niu, T. Tang, L.-B. Huang, Y.-Y. Chen, Z. Wei, J.-S. Hu, Self-terminated activation for high-yield production of N,P-codoped nanoporous carbon as an efficient metal-free electrocatalyst for Zn-air battery. *Carbon*, 2018, **128**, 97-105.

20 V. Kashyap, S. Kurungot, Zirconium-Substituted Cobalt Ferrite Nanoparticle Supported N-doped Reduced Graphene Oxide as an Efficient Bifunctional Electrocatalyst for Rechargeable Zn–Air Battery, *ACS Catal.*, 2018, **8**, 3715-3726.

21 C. Lai, J. Wang, W. Lei, C. Xuan, W. Xiao, T. Zhao, T. Huang, L. Chen, Y. Zhu, D. Wang, Restricting Growth of Ni_3Fe Nanoparticles on Heteroatom-Doped Carbon Nanotube/Graphene Nanosheets as Air-Electrode Electrocatalyst for Zn–Air Battery, *ACS Appl. Mater. Interfaces*, 2018, **10**, 38093-38100.

22 L. Yang, X. Zeng, D. Wang, D. Cao, Biomass-derived FeNi alloy and nitrogen-codoped porous carbons as highly efficient oxygen reduction and evolution bifunctional electrocatalysts for rechargeable Zn-air battery, *Energy Storage Mater*, 2018, **12**, 277-283.

23 H. Yang, B. Wang, H. Li, B. Ni, K. Wang, Q. Zhang, X. Wang, Trimetallic Sulfide Mesoporous Nanospheres as Superior Electrocatalysts for Rechargeable Zn-Air Batteries, *Adv. Energy Mater.*, 2018, **8**, 1801839.

24 F. Kong, X. Fan, A. Kong, Z. Zhou, X. Zhang, Y. Shan, Covalent Phenanthroline Framework Derived FeS@Fe_3C Composite Nanoparticles Embedding in N-S-Codoped Carbons as Highly Efficient Trifunctional Electrocatalysts, *Adv. Funct. Mater.*, 2018, **28**, 1803973.

25 L. Cao, Z.-h Li, Y. Gu, D.-h Li, K.-m. Su, D.-j. Yang, B.-w. Cheng, Rational design of N-doped carbon nanobox-supported $Fe/Fe_2N/Fe_3C$ nanoparticles as efficient oxygen reduction catalysts for Zn–air batteries, *J. Mater. Chem. A*, 2017, **5**, 11340-11347.

26 C. Zhu, Z. Yin, W. Lai, Y. Sun, L. Liu, X. Zhang, Y. Chen, S.-L. Chou, Fe-Ni-Mo Nitride Porous Nanotubes for Full Water Splitting and Zn-Air Batteries, *Adv. Energy Mater.*, 2018, **8**, 1802327.

27 G. Chen, J. Zhang, F. Wang, L. Wang, Z. Liao, E. Zschech, K. Mullen, X. Feng, Cobalt-Based Metal-Organic Framework Nanoarrays as Bifunctional Oxygen Electrocatalysts for Rechargeable Zn-Air Batteries, *Chemistry-A European J.*, 2018, **24**, 18413-18418.

28 S. Zeng, X. Tong, S. Zhou, B. Lv, J. Qiao, Y. Song, M. Chen, J. Di, Q. Li, All-in-One Bifunctional Oxygen Electrode Films for Flexible Zn-Air Batteries, *Small*, 2018, **14**, e1803409.

29 Y. Qiao, P. Yuan, Y. Hu, J. Zhang, S. Mu, J. Zhou, H. Li, H. Xia, J. He, Q. Xu, Sulfuration of an Fe-N-C Catalyst Containing Fe_xC/Fe Species to Enhance the Catalysis of Oxygen Reduction in Acidic Media and for Use in Flexible Zn-Air Batteries, *Adv. Mater.*, 2018, **30**, e1804504.

30 Y. Jiang, Y.-P. Deng, J. Fu, D. U. Lee, R. Liang, Z. P. Cano, Y. Liu, Z. Bai, S. Hwang, L. Yang, D. Su, W. Chu, Z. Chen, Interpenetrating Triphase Cobalt-Based Nanocomposites as Efficient Bifunctional Oxygen Electrocatalysts for Long-Lasting Rechargeable Zn-Air Batteries, *Adv. Energy Mater.*, 2018, **8**, 1702900.

31 B. Q. Li, S. Y. Zhang, B. Wang, Z. J. Xia, C. Tang, Q. A. Zhang, Porphyrin covalent organic framework cathode for flexible Zn-air batteries, *Energy Environ. Sci.*, 2018, **11**, 1723-1729.

32 L. Yang, L. Shi, D. Wang, Y. Lv, D. Cao, Single-atom cobalt electrocatalysts for foldable solid-state Zn-air battery, *Nano Energy*, 2018, **50**, 691-698.

33 W. Zang, A. Sumboja, Y. Ma, H. Zhang, Y. Wu, S. Wu, H. Wu, Z. Liu, C. Guan, J. Wang, S. J. Pennycook, Single Co Atoms Anchored in Porous N-Doped Carbon for Efficient Zinc−Air Battery Cathodes, *ACS Catal.*, 2018, **8**, 8961-8969.

34 C. Guan, A. Sumboja, W. Zang, Y. Qian, H. Zhang, X. Liu, Z. Liu, D. Zhao, S. J. Pennycook, J. Wang, Decorating Co/CoN_x nanoparticles in nitrogen-doped carbon nanoarrays for flexible and rechargeable zinc-air batteries, *Energy Storage Mater.*, 2019, **16**, 243-250.

35 K. Kordek, L. Jiang, K. Fan, Z. Zhu, L. Xu, M. Mamun, Y. Dou, S. Chen, P. Liu, H. Yin, P. Rutkowski, H. Zhao, Two-Step Activated Carbon Cloth with Oxygen-Rich Functional Groups as a High-Performance Additive-Free Air Electrode for Flexible Zinc-Air Batteries, *Adv. Energy Mater.*, 2018, 1802936.

36 Z. Zhao, Z. Yuan, Z. Fang, J. Jian, J. Li, M. Yang, C. Mo, Y. Zhang, X. Hu, P. Li, S. Wang, W. Hong, Z. Zheng, G. Ouyang, X. Chen, D. Yu, In Situ Activating Strategy to Significantly Boost Oxygen Electrocatalysis of Commercial Carbon Cloth for Flexible and Rechargeable Zn-Air Batteries, *Adv. Sci.*, 2018, **5**, 1800760.